Biochemistry and Biophysics Reports 41 (2025) 101901

Contents lists available at ScienceDirect

Biochemistry and Biophysics Reports

journal homepage: www.elsevier.com/locate/bbrep

Computational identification of novel natural inhibitors against triple mutant DNA gyrase A in fluoroquinolone-resistant *Salmonella* Typhimurium

Sree Haryini, George Priya Doss C *

Department of Integrative Biology, School of Biosciences and Technology, Vellore Institute of Technology (VIT), Vellore, 632014, Tamil Nadu, India

ARTICLE INFO

Keywords:
Fluoroquinolone resistance
Triple mutant
DNA gyrase A
Virtual screening
Salmonella Typhimurium

ABSTRACT

The rising resistance to fluoroquinolones in *Salmonella* Typhimurium poses a significant global health challenge. This computational research addresses the pressing need for new therapeutic drugs by utilizing various computational tools to identify potential natural compounds that can inhibit the triple mutant DNA gyrase subunit A enzyme, which is crucial in fluoroquinolone resistance. Initially, the three-dimensional structure of the wild-type DNA gyrase A protein was modeled using homology modeling, and followed by *in silico* mutagenesis to create the clinically relevant triple mutant (SER83PHE, ASP87GLY, ALA119SER) DNA gyrase A protein structure. The structural stability and integrity of the modeled protein were ensured through rigorous validation. Subsequently, a high-throughput virtual screening of a curated library of natural compounds was conducted to identify potential inhibitors against wild-type and triple-mutant proteins. The selected potent lead molecules comprehensively evaluated their physicochemical properties, ADME/T properties, and binding affinities via ADME/T assessment and molecular docking studies. The safest and most promising ligands were chosen for dynamics studies to analyze their dynamic behavior and protein stability before and after the binding of ligands. Our results showed that the natural compounds from the ChemDiv database, CID: 0407–0108, N039-0003, 1080–0568, and 0099–0261 have binding energies ranging from −4.32 to −5.69 kcal/mol and exhibit excellent physio-chemical properties, affinities, and are stable in their dynamic environments over 100 ns for both wild-type and triple mutant DNA gyrase A complexes. These compounds provide a promising alternative treatment for fluoroquinolone-resistant *Salmonella* Typhimurium infections.

1. Introduction

Gastroenteritis and invasive non-typhoidal fever, triggered by the gram-negative, enteric pathogen *Salmonella enterica* serovar Typhimurium, pose a significant global health risk in developed and developing nations, affecting animals and humans [1]. *Salmonella* is responsible for 25 % of all diarrheal diseases, with serovar Typhimurium being the most common and a significant contributor to foodborne infection outbreaks [2]. The severity of salmonellosis can range from mild to life-threatening, depending on various factors such as the severity of infestation, the microbial load ingested from contaminated food or other environmental sources, and the strength of the host's immune system [3]. The situation is further complicated by the lack of effective vaccines and the ongoing development of resistance against multiple first and second-generation antibiotic classes due to the acquisition of resistance genes and mutations in drug-binding sites. The 2022 outbreak of non-typhoidal infection caused by an unusual multidrug-resistant *Salmonella* Typhimurium (*S.* Typhimurium) strain has raised significant public health concerns worldwide [4]. Over the past decade, numerous strains of *S.* Typhimurium have developed resistance to multiple conventional antibiotics such as penicillin, fluoroquinolones, cephalosporins, carbapenems, and macrolides. This has led to the emergence of multi-drug-resistant (MDR) strains in countries like Malaysia, India, Vietnam, Indonesia, Thailand, and Pakistan [5–7]. In the late 1980s, fluoroquinolone drugs were prescribed for enteric and systemic fever as the number of MDR strains of *Salmonella* serovars, including Typhimurium serovar, increased. By the 2010s, subsequent resistance against cephalosporins, fluoroquinolones, tetracycline, and sulfamethoxazole emerged due to mutations and plasmid-mediated resistance, leading to increased resistance among *S.* Typhimurium strains [8].

Fluoroquinolone antibiotics, recognized for their broad spectrum, inhibit the activity of topoisomerase IV and DNA gyrase, thereby preventing DNA supercoiling during replication [9]. Although mutations in the DNA gyrase subunit B are less frequent compared to subunit A, both genes contribute to fluoroquinolone resistance [10]. Specifically,

* Corresponding author. Laboratory of Integrative Genomics, India.
E-mail addresses: sreeharyini.s2024@vitstudent.ac.in (S. Haryini), georgepriyadoss@vit.ac.in (G.P. Doss C).

https://doi.org/10.1016/j.bbrep.2024.101901
Received 7 November 2024; Received in revised form 13 December 2024; Accepted 13 December 2024

Abbreviation

WHO -	World Health Organisation
MDR -	Multi-drug-resistant
HTVS -	High Throughput Virtual Screening
SP -	Standard Precision
XP –	Extra Precision
RMSD -	Root Mean Square Deviation
RMSF -	Root Mean Square Fluctuation
Rg -	Radius of gyration
SASA -	Solvent Accessible Surface Area
H-bond -	Hydrogen bond
PCA -	Principal component analysis
FEL -	Free energy landscape
DCCM -	Dynamic Cross Correlation Matrix
MMPBSA -	Molecular Mechanics Poisson – Boltzmann Surface Area

mutations in the serine and aspartic acid residues at positions 83 and 87, respectively, within the quinolone binding site in the break reunion domain of the *gyrA* gene encoding DNA gyrase subunit A of *S.* Typhimurium are associated with fluoroquinolone resistance [11]. These residues are essential for fluoroquinolone binding, forming hydrogen bonds with water molecules and the Mg^{2+} ion complex, thereby hindering the resealing of DNA double-strand breaks [12]. Notably, the aspartic acid at position 87 of the *gyrA* gene plays a critical role in active binding and interaction with the positively charged nitrogen of fluoroquinolone antibiotics [13].

Clinical isolates from China have demonstrated double mutations in the *gyrA* gene and additional mutations in the *parC* gene at position 80 from serine to arginine. These mutations are significant as they considerably increase resistance to fluoroquinolone antibiotics, making infections more challenging to treat [14]. Studies from various geographical locations reported that the MDR- *Salmonella* serovars with double point mutations in *gyr*A subunit (SER 83 → PHE/TYR or ASP 87 → GLY/ASN) along with a *par*C single point mutation (SER 80 → ARG) exhibited ciprofloxacin resistance with minimum inhibitory concentration ranging > 0.5 mg/L [15–17]. A clinical strain of *S.* Typhimurium with a Minimum Inhibitory Concentration (MIC) of 512 mg/L isolated in the Middle East showed increased ciprofloxacin resistance due to a triple mutation in the *gyrA* gene alone (SER83PHE, ASP87GLY, ALA119SER), raising concerns about complete resistance to fluoroquinolones [18]. Therefore, bacteria's susceptibility to quinolones varies depending on the position of the mutation, the type of mutated amino acid, and the number of point mutations, altering the binding affinity of the DNA gyrase subunits in forming a complex with quinolone drugs. The prevalence of mutant strains with high fluoroquinolone resistance has notably increased in developing countries such as China, Thailand, Japan, India, Vietnam, Pakistan, Spain, and other Middle Eastern countries [18–20]. Given the organism's increasing complexity and resistance to multiple conventional drugs, developing new drugs structurally distinct from conventional ones is crucial.

Drug-like compounds from natural products have long been instrumental in discovering and developing drugs against various infectious diseases [21]. Secondary metabolites in plants and other natural resources, such as polyphenols, flavonoids, tannins, and alkaloids, function as defense mechanisms against microbial infections [22]. Screening libraries, like the natural compound library from the ChemDiv database, provide unique and novel drug-like compounds derived from natural resources. This collection comprises 374 distinct compounds similar to physiologically active natural substances. It is intricately associated with the Semi-Natural Screening Library of ChemDiv database, which includes over 16,500 substances. Consequently, rather than screening the 16,500 compounds, we focused only on the 374 compounds that exhibit superior similarity and biological activity. This accelerates the drug discovery process and assists in developing effective drugs against resistant pathogens that are less harmful to humans [22,23]. Despite numerous studies introducing bio-lead molecules with potential antibacterial activity, it is essential to screen these small molecules based on their drug-likeness, binding affinity, and dynamic behavior with the target protein. This is crucial for formulating novel drugs with enhanced efficacy compared to conventional ones.

The *in silico* study was designed to analyze the impact of the triple mutation on the DNA gyrase A protein structure and drug binding affinity with conventional drugs, which has not yet been explored computationally except for its occurrence in fluoroquinolone-resistant *S.* Typhimurium strains.The high-throughput computational screening of natural drug-like compounds was conducted to identify novel drug-like molecules capable of inhibiting DNA gyrase A wild-type (WT) and triple mutant (TM). Various computational tools were employed to study WT and TM proteins' dynamics, mutational stability, and binding affinity with novel natural phytochemical drug-like compounds.

2. Materials and methods

2.1. Target protein and ligand retrieval

The amino acid sequence information for the WT DNA gyrase subunit A protein of *S.* Typhimurium was retrieved from the Uniprot database (Uniprot ID: P37411) [24]. From the commercially accessible ChemDiv Natural compound database, 374 natural small molecules are in SDF format. This selection was based on their structural diversity and inherent bioactivity, which increases the likelihood of identifying effective inhibitors against fluoroquinolone-resistant DNA gyrase A of *S.* Typhimurium. Natural drugs are vital due to their optimized biological activity and favorable safety profiles. Furthermore, we obtained the 3D conformation of the control drug ciprofloxacin (PubChem ID: 2764) from the PubChem database [25].

2.2. Homology modeling and structure validate

Due to the lack of a three-dimensional (3D) crystal structure for DNA gyrase subunit A of *S.* Typhimurium, the breakage reunion domain of the DNA gyrase subunit A amino acid sequence from position 17 to 524 was modeled using the SWISS-MODEL server [26]. We selected a template structure from the Protein Data Bank (PDB) [27] or Alpha Fold [28] based on high GMQE, sequence similarity, and QSQE scores. This predicted a 3D protein structure, which served as the template for our modeling process [29]. Following this, the Prime module of Schrodinger [30] corrects the wrong angles and torsion angles of the modeled WT DNA gyrase subunit A protein structure. They optimized it by minimizing energy through the loop refinement tool. The resulting protein structure was evaluated for stability using MolProbity, confirmed by Ramachandran plot analysis.

2.3. Mutagenesis

The mutation information for the DNA gyrase subunit A of *S.* Typhimurium from the public database "DRAGdb: Drug Resistance Associated Genes" and relevant scholarly sources [18,31]. The computational method is vital for simulating mutations at specific amino acid sites, critical to studying protein mutations and developing drugs targeting mutant proteins. To introduce mutations and carry out computational mutagenesis, the Mutagenesis Wizard of the PyMOL molecular analysis visualization software was utilized [32].

2.4. Mutational protein stability analysis

The stability of a mutated protein is evaluated using DDMut, a

predictive tool specifically designed to analyze the stability of proteins that have undergone single or multiple-point mutations. DDMut employs a deep learning pipeline to predict changes in protein stability by calculating the Gibbs free energy changes associated with mutations. This tool enables quick and accurate assessments of the stabilizing and destabilising effects caused by mutations. For this study, DDMut was selected due to its strong capability to manage a variety of mutation scenarios, providing precise predictions crucial for understanding the impact of specific mutations on protein stability. The process involves feeding the WT protein structure and the intended mutations into DDMut, which then calculates the ΔΔG values to indicate whether a mutation stabilizes or destabilizes the protein. This quantitative analysis is vital for correlating the impacts of mutations with observed changes in the protein's function or behavior [33].

2.5. High throughput virtual screening

The ligand-receptor binding affinity of the DNA gyrase A protein is predicted using Schrodinger Glide software, which provides a broad range of applications, including binding mode prediction, virtual screening, and 3D molecular designing with an interactive interface [30]. Natural small molecules were prepared and assessed for drug-likeness and ADME/T properties based on the Lipinski rule using the QIKPROP tool in Schrodinger Maestro. This step facilitated filtering of active, potent, and inactive compounds [34]. Based on the proteins' geometry and topology, the active binding sites of the target protein were predicted using the CASTp 3.0 webserver [35]. A Grid file encompassing the protein's binding site was generated using the Grid generation panel in Glide Maestro. Computational screening of natural small molecules against the WT and TM proteins of *S.* Typhimurium was performed using the tri-docking mode of the Glide module. These include high throughput virtual screening (HTVS), which is the fastest and least precise mode; standard precision (SP) docking, offering moderate speed and precision; and extra-precision (XP) docking, the slowest but most precise docking mode [36]. Initially, HTVS was used to screen a large number of compounds swiftly. The top hits from HTVS were then subjected to SP docking for more accurate predictions, and the best candidates from SP docking were further refined using XP docking to obtain the most precise binding affinities and interactions. The top four natural drug-like compounds from the XP results, which demonstrated the best docking and glide scores, were selected for further analysis and visualization. Additionally, the WT and TM proteins were docked with the control drug ciprofloxacin using the XP docking mode to obtain precise binding energy results for comparison. The interactions of the top compounds with their respective target proteins and the control drug with the WT/TM proteins were visualized using the Ligand interaction tool in Schrodinger Maestro. Moreover, the 3D interactions of the docked poses of these complexes were visualized using the ChimeraX visualization tool [37].

2.6. Molecular dynamic simulation

The interatomic interactions and dynamics of the top screened compounds and the control drug-DNA gyrase WT and TM protein complexes were studied over 100ns using GROMACS version 2023 [38]. The starting poses for the ligands were taken from the best-docked conformations obtained from the preceding docking studies. Input files for the GROMACS simulation of DNA gyrase WT/MT protein-ligand complexes were prepared using the CHARMM-GUI solution builder model in a water-based solvent [39]. The ligand-receptor complexes were solvated and neutralized with water molecules and Na^+ and Cl^- ions at physiological concentrations of 0.15 M, automatically estimated based on the system's net charge and ion-accessible volume (V). Periodic boundary conditions were applied to the rectangular solvation box according to the dimensions of the complex. The PME method (Particle Mesh Ewald) handled long-range electrostatic interactions, and energy minimization of the complexes was performed for 50,000 steps to eliminate unfavorable contacts. The LINCS algorithm was used for the GROMACS inputs. The solvated complexes underwent equilibration under default NVT (constant volume and temperature) conditions for 100 ps, followed by NPT (constant pressure and temperature) conditions for another 100 ps [40]. Various standard parameters such as Root Mean Square Deviation (RMSD), Root Mean Square Fluctuation (RMSF), Radius of gyration (Rg), Solvent Accessible Surface Area (SASA), Hydrogen bond analysis, Principal component analysis (PCA), Free energy landscape (FEL), and Dynamic Cross Correlation Matrix (DCCM) were used to analyze the trajectory of the 100 ns simulation of the complexes. Trajectory file outcomes were plotted using QtGrace software better to understand the dynamics of the protein-ligand complex interactions.

2.6.1. Principal component analysis (PCA)

PCA was employed to analyze the collective motions and substantial fluctuations at the atomic level in the WT and TM with ligand complexes. The eigenvalues, eigenvectors, and their projections were assessed to analyze the principal components of the target proteins. The principal components 1 (PC1) and 2 (PC2) were selected to examine significant atomic motions in the target-ligand complexes. Higher stability of the target protein-ligand complex is indicated by the complex occupying less phase than the stable cluster, and vice versa [41].

2.6.2. Free energy landscape (FEL) analysis

The molecular free energy and their biomolecular folding and interaction were analyzed and interpreted using the free energy landscape, which was estimated using the formula;

$$\Delta G\alpha = -K_B T \ln\left[\frac{P(q\alpha)}{Pmax\ (q)}\right]$$

Here, T represents the simulation temperature, K_B represents the Boltzmann constant, (qα) represents the estimated probability density function derived from molecular dynamics histogram data, and Pmax (q) represents the probability of the possible state. The 2D free energy landscapes were obtained from the combined probability distributions of the complex system's q_i and q_j reaction coordinates [42].

2.6.3. Dynamic cross-correlation matrix (DCCM)

The DCCM is a widely used trajectory analysis method in dynamic simulation, which analyses the multi-correlated motion and behaviors of alpha carbon atoms in the target proteins. The coordinates and configurations of the backbone C_α atoms before and after ligand interaction are calculated using the least-square fitting method and then graphically visualized [43]. The DDCM analysis is carried out using the following technical formula:

$$DCCM_{(i,j)} = \frac{\langle \Delta ri X \Delta rj \rangle}{\sqrt{\langle \Delta ri^2 \rangle}\sqrt{\langle \Delta rj^2 \rangle}}$$

Here, $\Delta r_{i,\,j}$ represents the average movement of the proteins' i^{th} and j^{th} atoms. The value of C_{ij} ranges from −1 to 1, where 1 indicates correlated atom movement, while −1 indicates highly anti-correlated movement.

2.7. Molecular mechanics Poisson – Boltzmann surface area (MMPBSA)

The free binding energy between the interacting target and ligand was calculated using the g_MMPBSA tool, an open-source drug consortium [44]. The calculation was performed with the last 25 ns of every simulation of best-docked complexes of ligands with WT and TM DNA gyrase subunit A of *S.* Typhimurium to evaluate the stability of the interaction between the target WT and TM proteins and the selected ligands. The following mathematical equation is crucial to understanding and determining the free binding energies. The difference between

the complex free energy ($\Delta G_{complex}$) and the sum of target protein free energy and ligand-free energy ($\Delta G_{protein} + \Delta G_{ligand}$) gives the total free binding energy ($\Delta G_{binding}$) [45].

$$\Delta G_{binding} = \Delta G_{complex} - (\Delta G_{protein} + \Delta G_{ligand})$$

The mean potential energy of the complexes in vacuum condition (ΔEMM) and their entropic involvement at the kelvin temperature T, respectively, were determined by the mathematical formula:

$$\Delta G_{binding} = \Delta E_{MM} - T\Delta S + T\Delta S_{sol}$$

$$\Delta E_{MM} = \Delta E_{ele} + \Delta E_{vdw}$$

The combined total value of electrostatic and non-electrostatic forces gives the solvation energy ($G_{solvation}$), which can be represented as an equation:

$$G_{solvation} = G_{polar} + \Delta G_{nonpolar}$$

The Poisson—Boltzmann linear formula calculates polar solvation energy, whereas non-polar solvation energy can be computed using solvent-accessible surface area (SASA).

$$G_{polar} = \gamma SASA + \beta$$

MM-PBSA analysis aids in estimating each residue's contribution to the complex's total binding energy.

3. Result

3.1. Homology modeling and protein structure validation

The break reunion domain of DNA gyrase subunit A (position: 17 to 524) from *S.* Typhimurium was modeled using the homology of the template structure from the AlphaFold model, which had a GMQE score of 0.94 and 100 % identity (Template ID: AlphaFold DB model of A0A659S2X5_SALET), as per the SWISS-MODEL template prediction result. MolProbity, a widely recognized protein structure validation web server, was employed to evaluate the stability of the modeled protein structure through the Ramachandran Plot. The analysis of the modeled WT DNA gyrase subunit A revealed a MolProbity clash score of 0.67, with 97.07 % of the residues in the Ramachandran favored region and 0.20 % of the residues in the outliers, as per the results of the Ramachandran's plot depicted in Fig. S1. These results are significant as they indicate a highly accurate and stable model, essential for understanding the proteins' function and subsequent applications such as drug design. The high percentage of residues in the favored region suggests that the protein adopts a plausible and stable conformation akin to experimentally determined structures. The low clash score and minimal outliers further validate the model's reliability, providing confidence in using this model for further functional and interaction studies. Thus, these validations highlight the model's potential usefulness in biomedical studies and therapeutic development targeting *S.* Typhimurium.

3.2. Mutagenesis and protein stability

Mutation data related to fluoroquinolone resistance in DNA gyrase subunit A of *S.* Typhimurium was gathered from the DRAG database. Various literature sources indicated common mutations at position 83 (serine to phenylalanine), 87 (aspartic acid mutated to glycine), and 119 (alanine mutated to serine), which contributed to the increased fluoroquinolone resistance in *S.* Typhimurium. Using the Mutagenesis Wizard of PyMol software, point mutations were simulated at positions 83, 87, and 119 of DNA gyrase subunit A, including the TM in the target WT protein. The resulting TM structure was saved in. pdb format. The impact of these mutations on protein stability was then studied using DDMut. The mutational protein stability analysis of the TM protein revealed a destabilization with a ΔΔG value of −0.22 kcal/mol. Individual point mutations in the WT protein showed that the mutations at position 87 (aspartic acid to glycine) and 119 (alanine to serine) destabilized the protein with ΔΔG values of −0.55 and −0.15 kcal/mol, respectively. In contrast, the mutation at position 83 (serine to phenylalanine) stabilized the protein with an ΔΔG value of 0.03 kcal/mol. Table 1 represents the flexibility and stability of the mutated TM protein analysis by DDMut.

3.3. Virtual screening analysis

High throughput computational screening of natural drug-like small molecules was performed using the Glide suite of Schrodinger software. The process involved filtering the top natural compounds based on ADME/T and Lipinski rule criteria, followed by high-throughput and standard precision docking. Compounds with the best-docked and high glide scores were selected for further *in silico* analysis. After thorough scrutiny and filtration, the top four natural compounds with the best hit on WT and TM protein were chosen. The binding energies and interactions of the top-docked compounds with the WT protein are summarized as follows: Complex WT_0407–0108 exhibited a binding energy of −5.17 kcal/mol, interacting with ASP20, ARG30, ARG31, ASP131, ASP141 amino acid residues, forming five conventional polar H-bonds. Complex WT_N039-0003 exhibited a binding energy of −5.11 kcal/mol, interacting with HIS322 and GLU344, forming two conventional polar H-bonds. Complex WT_1080–0568 exhibited a binding energy of −4.44 kcal/mol, interacting with ARG349 and GLU353, forming four conventional polar H-bonds. The control drug complex, WT_Ciprofloxacin, exhibited a binding energy of −3.65 kcal/mol, interacting with LYS113 and ASP499, forming one conventional polar H-bond. Comparing the binding energies of the WT protein with the control drug and screened natural compounds, the top three docked natural compounds show higher potency in inhibiting the DNA gyrase activity of fluoroquinolone-sensitive *S.* Typhimurium strains. The binding energies and interactions of the top docked compounds with the TM protein were as follows: Complex TM_0407–0108 exhibited a binding energy of −5.69 kcal/mol, interacting with ASP66, ALA101 amino acid residues, forming four conventional polar H-bonds. Complex TM_N039-0003 exhibited a binding energy of −5.42 kcal/mol, interacting with HIS322 and GLU344 amino acid residues, forming two conventional polar H-bonds. Complex TM_ 0099–0261 exhibited a binding energy of −4.32 kcal/mol, interacting with ARG75, ASN149, and SER156, forming three conventional polar H-bonds. The control drug complex TM_Ciprofloxacin, exhibited a binding energy of −3.67 kcal/mol, interacting with LYS113 and ASP499 amino acid residue, forming two conventional polar H-bonds. Comparing the binding energies of the TM protein with the control drug and the screened natural compounds, the top three docked natural compounds appear to be more potent in inhibiting the DNA gyrase activity of fluoroquinolone-resistant *S.* Typhimurium strains. The 2D and 3D interaction of the WT and TM with their respective ligand small molecules were visualized using the Ligand interaction tool of the Maestro suite (Fig. 1) and ChimeraX visualization tool (Figs. 2 and 3). Table 2 comprehensively summarizes the docking results of WT and TM DNA gyrase subunit A protein of *S.* Typhimurium with the top screened drug-like natural compounds.

Table 1
Analysis of flexibility, and protein stability of the mutated triple mutant DNA Gyrase subunit A protein of *Salmonella* Typhimurium using DDMut.

	DDMut	
Mutant	delta G value (kcal/mol)	Stability of protein
SER83PHE	0.03	Stabilizing
ASP87GLY	−0.55	Destabilising
ALA119SER	−0.15	Destabilising
Triple Mutant	−0.22	Destabilising

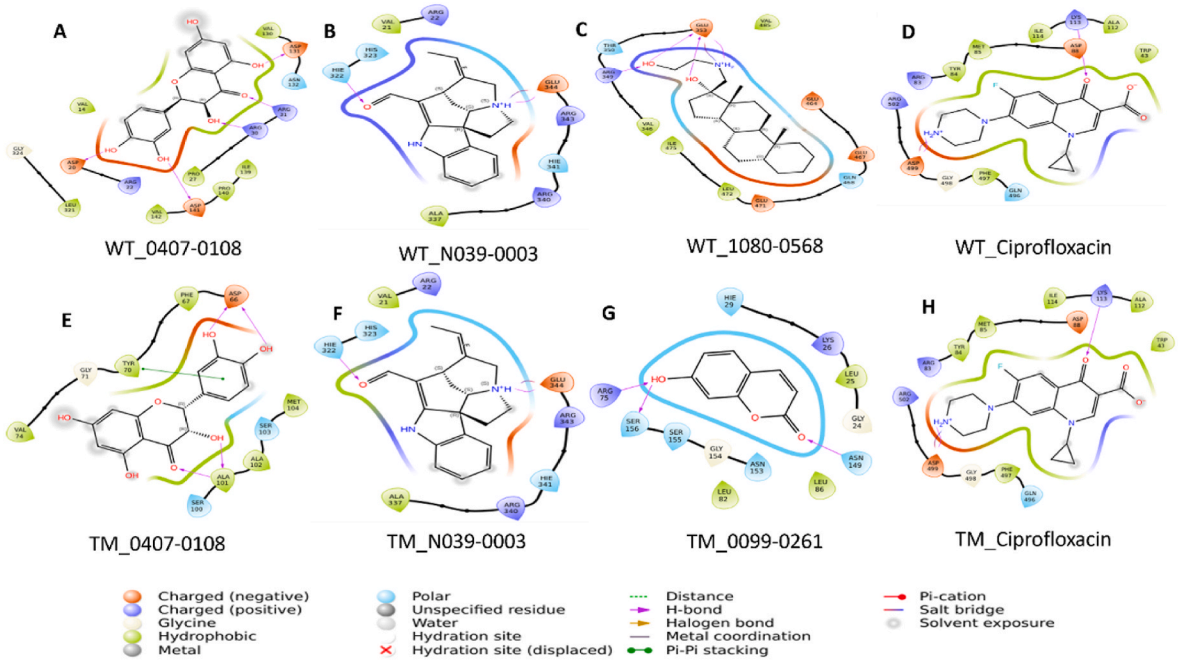

Fig. 1. 2D interaction of best-docked natural compounds and control drug with wild-type (WT) and triple mutant (TM) DNA gyrase A protein. 2D interactions of A) WT with ligand 0407–0108, B) WT with ligand N039–0003, C) WT with ligand 1080–0568, D) WT with ciprofloxacin, E) TM with ligand 0407–0108, F) TM with ligand N039-0003, G) TM with ligand 0099–0261, H) TM with ligand ciprofloxacin.

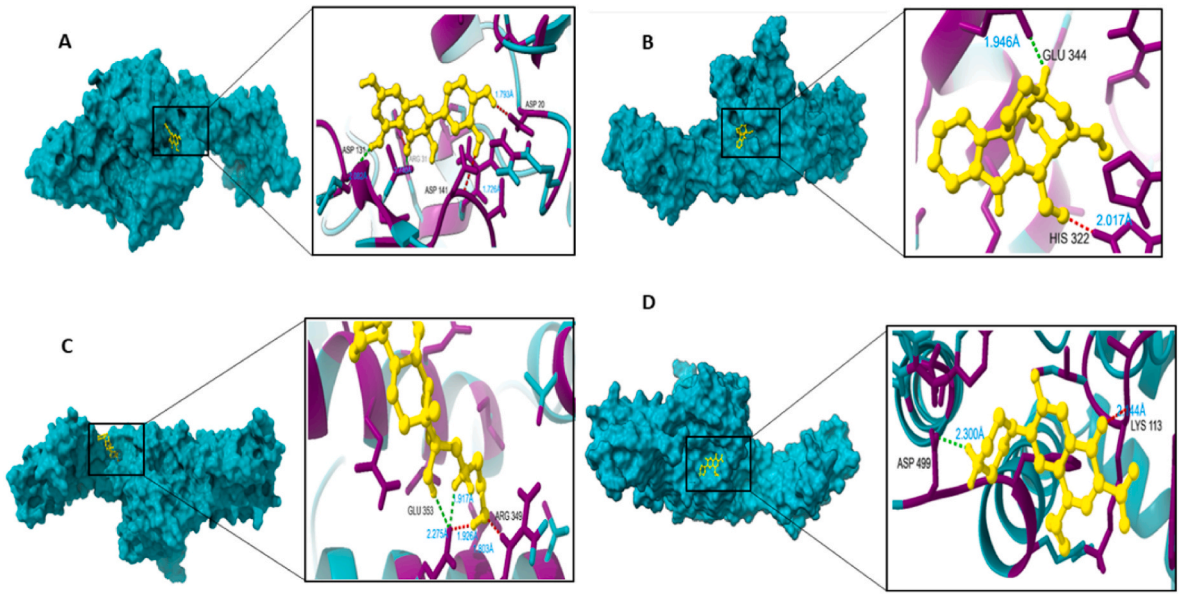

Fig. 2. 3D interaction of best-docked natural compounds and control drugs with wild-type (WT) DNA gyrase A protein. A) WT with ligand 0407–0108, B) WT with ligand N039–0003, C) WT with ligand 1080–0568, D) WT with ciprofloxacin.

3.4. ADME/T and physio-chemical properties of screened compounds

The pharmacokinetics, drug-likeness, and physicochemical properties of the chosen ligands were examined using the QIKPROP tool in Schrodinger Maestro. The ligands displayed a molecular weight ranging from 162.14 g/mol to 349.55 g/mol, with the ability to donate 1 to 5 H-bonds and accept 2 to 7 H-bonds each. Moreover, the topological polar surface area of the top four screened compounds ranged from 32.34 Å^2 to 127.45 Å^2. Table 3 provides a summary of the physicochemical properties of the top four drug-like compounds 0407–0108, N039-0003, 1080–0568, and 0099–0261, offering insights into their ADME/T properties, including BBB (blood-brain barrier) and absorption characteristics. Lipophilicity, a crucial drug discovery and development parameter, was evaluated by calculating the partition coefficient between water and *n*-octanol (log Po/w). The hydrophobicity, lipophilicity (QPlogPC16, QPlogPoct), polarizability (QPpolrz), skin permeability (QPlog Kp), absorption and distribution (QPlogPw, QPlogPo/w, and QPlogS) of the selected ligands were analyzed using the QIKPROP tool of Schrodinger. All the chosen natural drug-like compounds successfully passed the ADME/T assessment, meeting the strict standard limits of QPpolz (13–70), QPlogPC16 (4–18), QPlogPoct (8–43), QPlogPw (5–48), QPlogPo/w (−2 to 6), QPlogS (−6 to 0.5) and Qplog Kp (−8 to

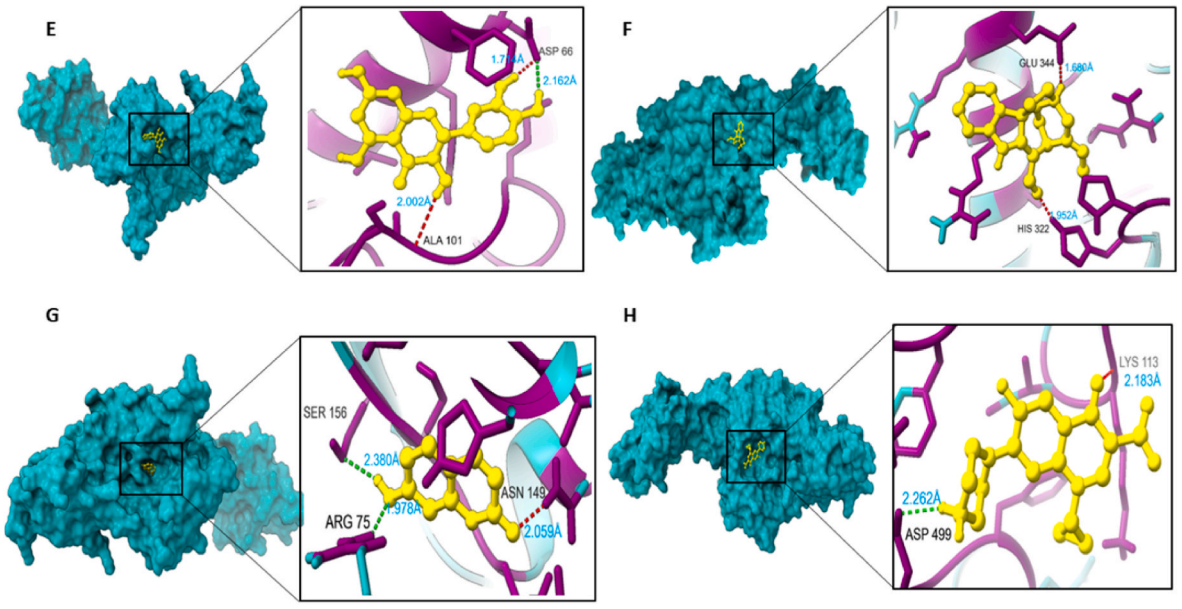

Fig. 3. 3D interaction of best-docked natural compounds and control drug with triple mutant (TM) DNA gyrase A protein. E) TM with ligand 0407–0108, F) TM with ligand N039–0003, G) TM with ligand 0099–0261, H) TM with ligand ciprofloxacin.

Table 2
It gives the docking, glide score outcomes and the interactive sites of natural compounds and control drug ciprofloxacin against the wild type and triple mutant protein of DNA gyrase subunit A of *Salmonella* Typhimurium respectively.

Target Protein	Compound Name/ID	Docking Score (kcal/mol)	Glide G-score	Glide E-model	XP G-Score	Interactive sites
Wild type	0407–0108	−5.17	−5.21	−51.60	−5.21	ASP20, ASP141, ARG30, ARG31, ASP131
	N039-0003	−5.11	−5.22	−45.10	−5.22	HIS322, GLU344
	1080–0568	−4.44	−4.45	−44.671	−4.45	ARG349, GLU353
	Control drug- Ciprofloxacin	−3.65	−3.76	−43.58	−3.76	LYS113, ASP499
Triple mutant	0407–0108	−5.69	−5.73	−43.11	−5.73	ASP66, ALA101
	N039-0003	−5.42	−5.53	−44.82	−5.53	HIS322, GLU344
	0099–0261	−4.32	−4.33	−34.175	−4.33	ARG75, SER156, ASN149
	Control drug- Ciprofloxacin	−3.67	−3.78	−43.37	−3.78	LYS 113, ASP499

Table 3
Physio-chemical properties of top 4 screened drug-like compounds of extra precision docking outcome.

Natural compounds	Structure	X logP	Molecular weight (g/mol)	H-bond donors	H-bond acceptors	Tpsa (Å^2)	Rotatable bonds
0407–0108	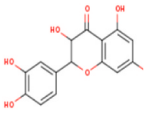	0.95	304.25	5	7	127.45	1
N039-0003	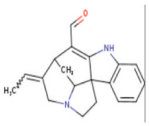	1.98	292.37	1	2	32.34	1
1080–0568	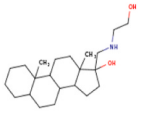	4.60	349.55	3	3	52.49	4
0099–0261	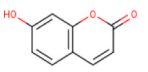	1.58	162.14	1	3	50.44	0

−1). Table 4 represents the ADME/T properties of these selected novel natural drug-like compounds. Therefore, based on the collective ADME/T property data of the selected compounds, we can infer that these proposed compounds are potentially safe and effective drug molecules against the target proteins.

Table 4
Absorption and distribution properties with standard limits of the top 4 hit compounds obtained from the docking analysis.

Natural compounds	QP polrz (13–70)	QPlogPC16 (4–18)	QPlogPoct (8-43)	QPlogPw (5-48)	QPlogPo/w (−2 to 6)	QPlogS (−6 to 0.5)	Qplog Kp (−8 to −1)
0407–0108	27.83	10.709	19.372	15.42	0.116	−2.731	−5.407
N039-0003	32.344	8.863	12.297	5.393	3.08	−3.059	−4.326
1080–0568	37.11	10.453	18.13	8.77	3.517	−3.789	−4.575
0099–0261	16.837	6.032	9.997	7.343	0.719	−1.434	−2.997

3.5. Dynamic trajectory analysis

3.5.1. Root Mean Square Deviation (RMSD)

RMSD trajectories provide valuable insights into the flexibility and stability of the protein-ligand complex during MDS. Fig. 4 depicts the structural deviation of the WT and TM protein-ligand complexes throughout 100 ns. The RMSD graph of WT_0407–0108 and TM_0407–0108 complex (Fig. 4A) displays an initial convergent fluctuation from 0.1 nm to approximately 0.35 nm until 35 ns, after which they stabilize. The average RMSD values of WT_0407–0108 and TM_0407–0108 complexes were 0.252 ± 0.035 nm and 0.225 ± 0.034 nm, respectively. RMSD graph of WT_N039-0003 and TM_N039-0003 complex (Fig. 4B) exhibited a gradual increase in fluctuation until 12 ns, ranging from 0.1 nm to around 0.3 nm, followed by stabilization until 50 ns. Beyond 50 ns, there is a notable fluctuation in WT_N039-0003 from 0.2 nm to approximately 0.45 nm compared to TM_N039-0003 until 75 ns, after which both complexes stabilize. The average RMSD values of WT_N039-0003 and TM_N039-0003 complexes were 0.258 ± 0.066 nm and 0.225 ± 0.041 nm, respectively. Examining the comparative RMSD graph of the ciprofloxacin control drug in complex with WT and TM protein (Fig. 4C), minimal fluctuation from 0.2 nm to around 0.35 nm is observed throughout the simulation. However, after 75 ns, there is a sudden drop in the RMSD value of the TM_Ciprofloxacin complex from 0.25 nm to 0.15 nm, followed by an increase to 0.30 nm. The mean RMSD values of WT_Ciprofloxacin and TM_Ciprofloxacin were 0.240 ± 0.039 nm and 0.220 ± 0.042 nm, respectively. Fig. 4D displays the RMSD graph of complexes WT_1080–0568 and TM_0099–0261, respectively. Both complexes fluctuated from 0.150 nm to 0.38 nm, with consistent protein stabilization observed. The mean RMSD values of WT_1080–0568 and TM_0099–0261 were 0.225 ± 0.032 nm and 0.208 ± 0.038 nm, respectively.

3.5.2. Root Mean Square Fluctuation (RMSF)

RMSF measures the average deviation of each amino acid residue in a protein over a 100 ns simulation period from its reference position, thereby corroborating the RMSD results. Fig. 5A illustrates the RMSF profile of the Cα backbone for the WT_0407–0108 and TM_0407–0108 complexes, revealing variable RMSF values across different residues. A pronounced fluctuation peak around the 100th residue, particularly in the WT protein, suggests increased flexibility. Significant peaks are observed around residues 237, 260–300, 360–400, and a notable peak near residue 500 in the TM complex. The average RMSF for the WT_0407–0108 and TM_0407–0108 complexes are 0.146 ± 0.089 nm and 0.139 ± 0.084 nm, respectively. In the comparative RMSF graph for the WT_N039-0003 and TM_N039-0003 complexes (Fig. 5B), a significant peak at the 100th residue is noted in the TM_N039-0003 complex but not in the WT_N039-0003. Similar to the WT_0407–0108 and TM_0407–0108 complexes, peaks are observed around residues 237, 260–300, 360–400, and near residue 500. The average RMSF values for WT_N039-0003 and TM_N039-0003 are 0.148 ± 0.094 nm and 0.141 ± 0.089 nm, respectively. The RMSF graph for WT_Ciprofloxacin and TM_Ciprofloxacin (Fig. 5C) shows similar fluctuating peaks at residues

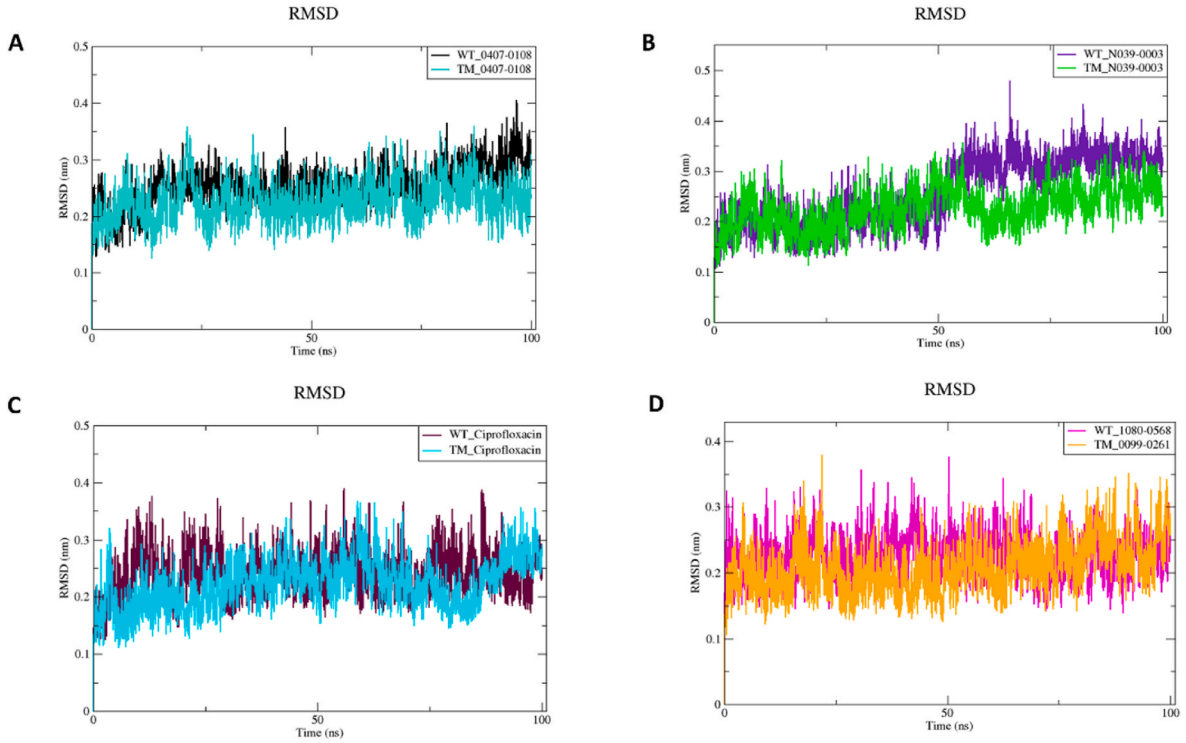

Fig. 4. RMSD analysis of all complexes. A) Comparative RMSD graph of WT and TM in complex with ligand 0407–0108, B) Comparative RMSD graph of WT and TM in complex with ligand N039–0003, C) Comparative RMSD graph of WT and TM in complex with Ciprofloxacin, D) Comparative RMSD graph of complex WT with ligand 1080–0568 and TM with ligand 0099–0261.

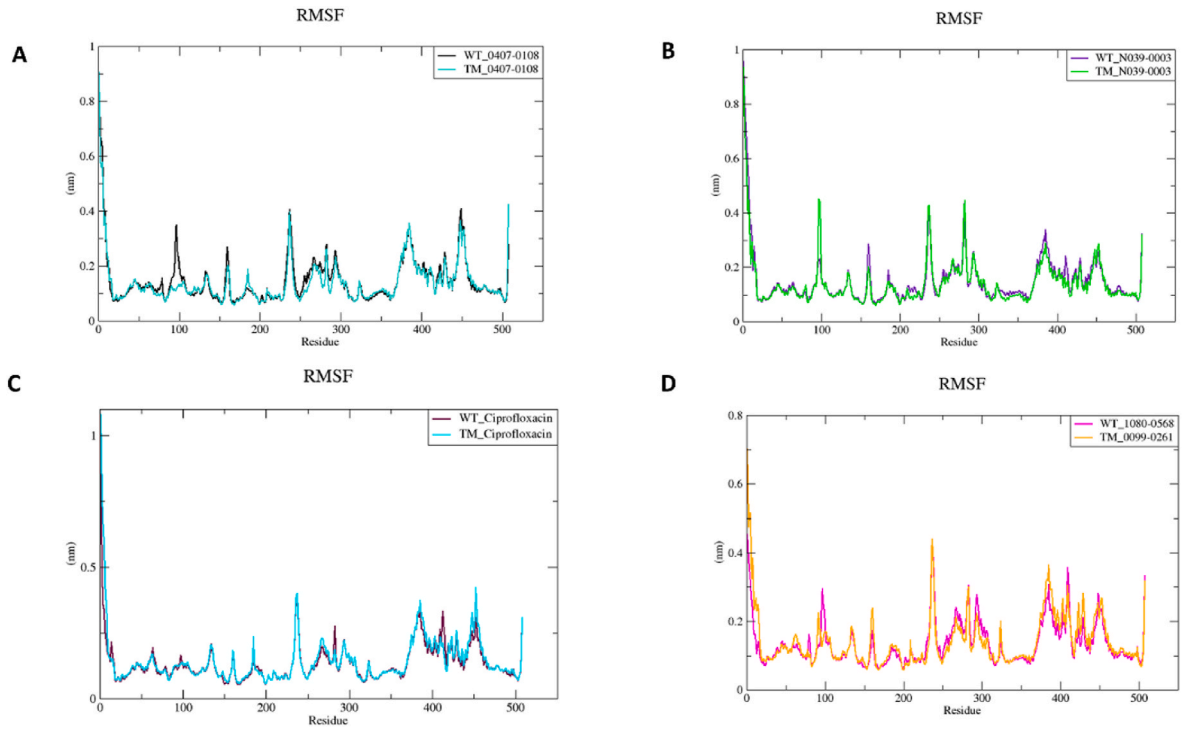

Fig. 5. RMSF analysis of all complexes. A) Comparative RMSF graph of WT and TM in complex with ligand 0407–0108, B) Comparative RMSF graph of WT and TM in complex with ligand N039–0003, C) Comparative RMSF graph of WT and TM in complex with Ciprofloxacin, D) Comparative RMSF graph of complex WT with ligand 1080–0568 and TM with ligand 0099–0261.

237, 260–300, 360–400, and near residue 500, but no significant fluctuation at the 100th residue. The mean RMSF values for WT_Ciprofloxacin and TM_Ciprofloxacin are 0.136 ± 0.074 nm and 0.143 ± 0.095 nm, respectively. Conversely, the RMSF graph for the WT_1080–0568 and TM_0099–0261 complexes (Fig. 5D) displays similar significant peaks at the same positions, except at the 100th residue, where a notable peak is observed only in the WT_1080–0568 complex, akin to the WT_0407–0108 and TM_N039-0003 graphs. The

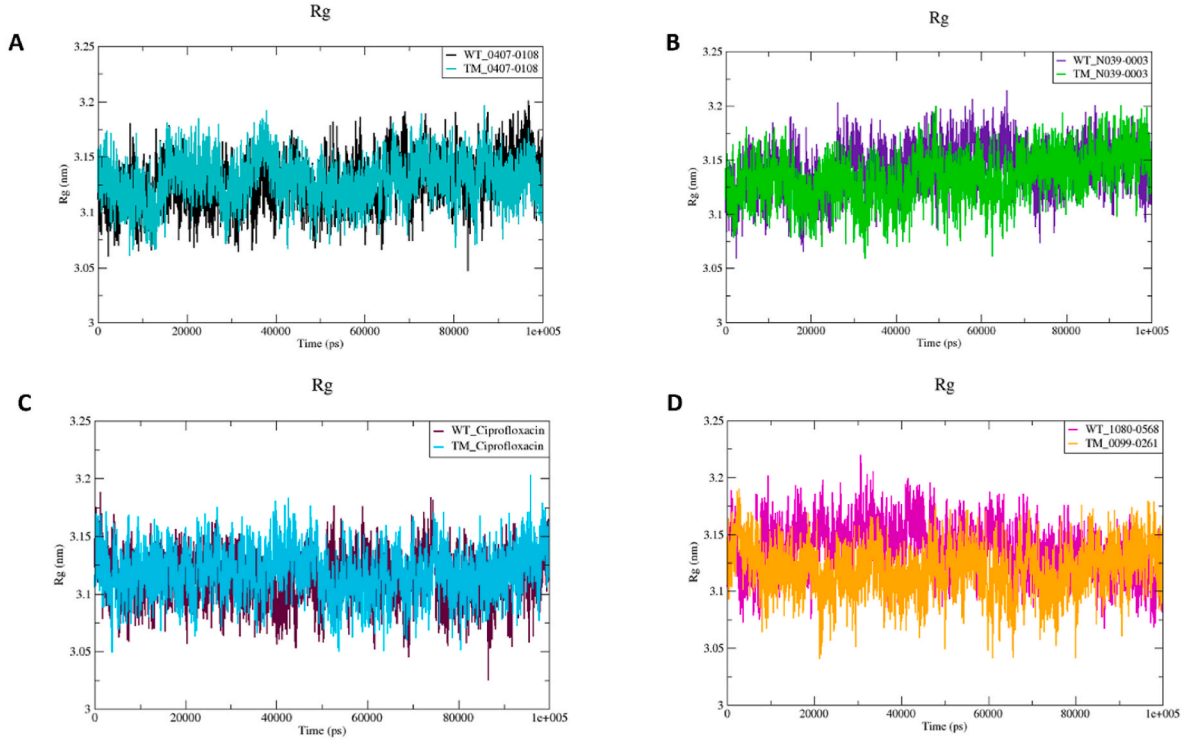

Fig. 6. Rg analysis of all complexes. A) Comparative Rg graph of WT and TM in complex with ligand 0407–0108, B) Comparative Rg graph of WT and TM in complex with ligand N039–0003, C) Comparative Rg graph of WT and TM in complex with Ciprofloxacin, D) Comparative Rg graph of complex WT with ligand 1080–0568 and TM with ligand 0099-0261.

average RMSF values for WT_1080–0568 and TM_0099–0261 are 0.136 ± 0.074 nm and 0.141 ± 0.077 nm, respectively.

3.5.3. Radius of gyration (Rg)

The Rg is essential for evaluating protein-ligand complexes' compactness and structural integrity during simulations. Fig. 6 illustrates the Rg values for all complexes, highlighting the compactness of wild-type (WT) and mutant (TM) proteins when bound to various ligands. The Rg values range from approximately 3.05 nm–3.2 nm, indicating minor variations in compactness across different complexes. The average Rg values for the WT_0407–0108 and TM_0407–0108 complexes were 3.126 ± 0.021 nm and 3.128 ± 0.019 nm, respectively. These similar values suggest that WT and TM proteins maintain comparable compactness when interacting with ligands 0407–0108. Slightly higher average Rg values were observed for the WT_N039-003 (3.14 ± 0.020 nm) and TM_N039-0003 (3.13 ± 0.020 nm) complexes, indicating a marginally less compact structure compared to the 0407–0108 complexes, though the difference is minimal. The average Rg values for the control drug ciprofloxacin were 3.11 ± 0.019 nm for WT_Ciprofloxacin and 3.12 ± 0.019 nm for TM_Ciprofloxacin. These values fall within the typical range observed for other complexes, suggesting that ciprofloxacin does not significantly alter the compactness of the protein-ligand complexes. The average Rg values for the WT_1080–0568 and TM_0099–0261 complexes were 3.136 ± 0.02 nm and 3.118 ± 0.02 nm, respectively. These results demonstrate a consistent pattern of compactness, reinforcing the structural stability of both WT and TM proteins across different ligand interactions. The Rg analysis indicates that WT and TM proteins exhibit similar compactness when bound to various ligands, with only minor variations observed. This consistency suggests that the mutations present in TM proteins do not significantly impact the overall compactness and stability of the protein-ligand complexes.

3.5.4. Solvent accessible surface area (SASA)

The SASA quantifies the protein surface area exposed to a solvent, such as water, providing insights into the hydrophobic and hydrophilic characteristics of the complex. Fig. 7 displays the SASA trajectory analysis for all complexes. The average SASA values for the WT_0407–0108 and TM_0407–0108 complexes were 260.10 ± 3.502 nm^2 and 258.88 ± 2.716 nm^2, respectively. For the WT_N039-0003 and TM_N039-0003 complexes, the average SASA values were 261.14 ± 2.99 nm^2 and 261.79 ± 3.149 nm^2, respectively. The WT_Ciprofloxacin and TM_Ciprofloxacin complexes had mean SASA values of 258.55 ± 3.05 nm^2 and 260.97 ± 3.32 nm^2, respectively. Additionally, the average SASA values for the WT_1080–0568 and TM_0099–0261 complexes were 261.84 ± 3.09 nm^2 and 263.18 ± 3.676 nm^2, respectively. These SASA values provide a comprehensive understanding of the surface exposure and interaction dynamics of the protein-ligand complexes, highlighting the subtle differences in hydrophobic and hydrophilic behavior across various complexes.

3.5.5. Hydrogen bond (H-bond) analysis

The evaluation of protein-ligand interactions, specifically their strength and stability, is conducted through H-bond analysis. The Y-axis quantifies the number of H-bonds formed between wild-type (WT) and mutant (TM) proteins with their respective ligands. The X-axis represents the simulation duration, set at 100 ns. Fig. 8 illustrates the H-bond analysis across all complexes. During the 100 ns simulation, WT_0407–0108 and TM_0407–0108 complexes formed four H-bonds. Conversely, the WT_N039-0003 and TM_N039-0003 complexes exhibited the formation of only two and one H-bonds, respectively. The WT_Ciprofloxacin and TM_Ciprofloxacin complexes formed four and three H-bonds, respectively. Additionally, the WT_1080–0568 complex formed three H-bonds, while the TM_0099–0261 complex formed two H-bonds.

3.5.6. Principal component analysis (PCA)

PCA was employed to evaluate the coordinated dynamic movements of the alpha carbon in both wild-type (WT) and mutant (TM) proteins when complexed with their respective ligands. This analysis utilized two

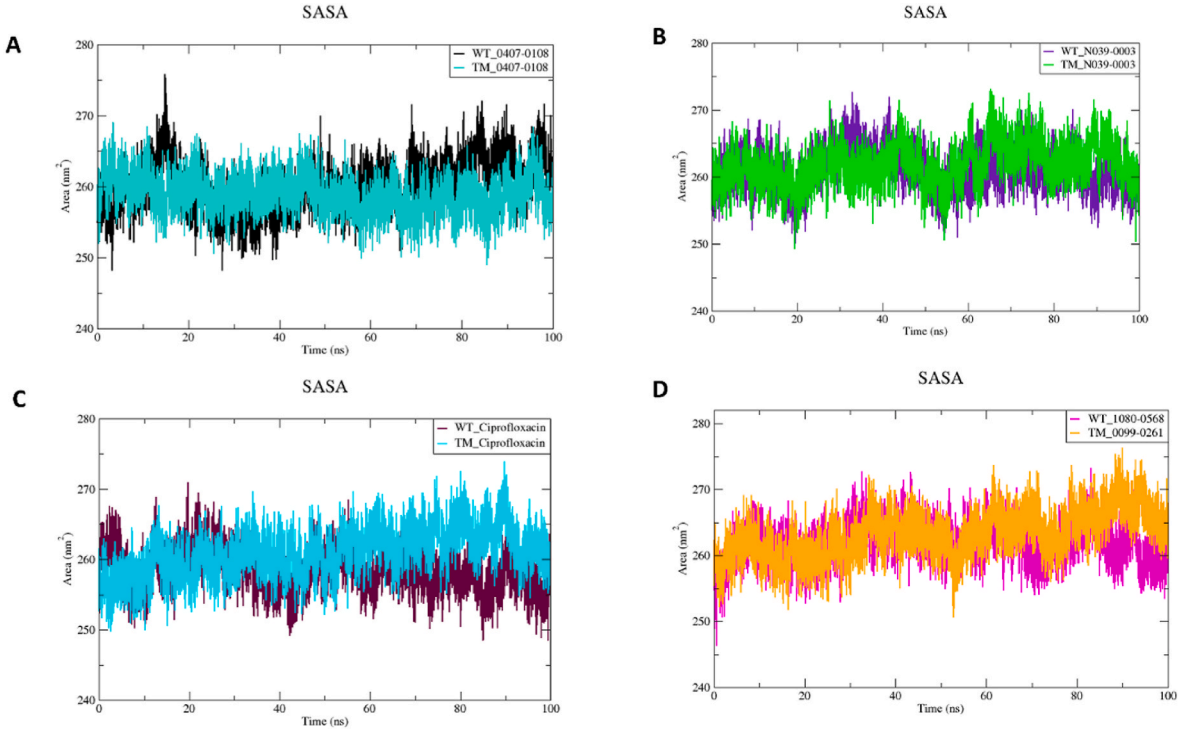

Fig. 7. SASA analysis of all complexes. A) Comparative SASA graph of WT and TM in complex with ligand 0407–0108, B) Comparative SASA graph of WT and TM in complex with ligand N039–0003, C) Comparative SASA graph of WT and TM in complex with Ciprofloxacin, D) Comparative SASA graph of complex WT with ligand 1080–0568 and TM with ligand 0099–0261.

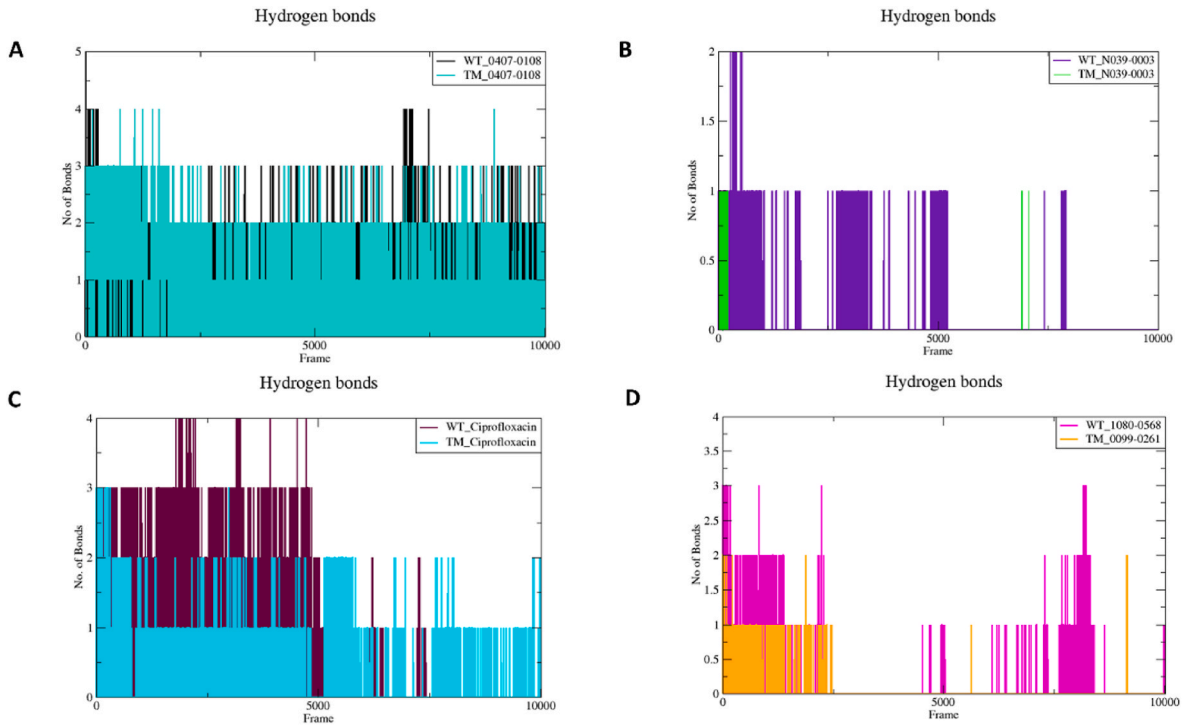

Fig. 8. Hydrogen bond analysis of all complexes. A) Comparative hydrogen bond analysis of WT and TM with ligand 0407–0108, B) Comparative hydrogen bond analysis of WT and TM with ligand N039–0003, C) Comparative hydrogen bond analysis of WT and TM with Ciprofloxacin, D) WT with ligand 1080–0568 and TM with ligand 0099–0261.

principal components (PC1 and PC2) and eigenvectors to determine the direction of variations. The 2-D trajectory projections of all complexes were plotted, with eigenvector one on the x-axis and eigenvector two on the y-axis, as shown in Fig. 9. Comparative analysis of the PCA plots for the complexes WT_0407–0108 with TM_0407–0108, WT_N039-0003 with TM_N039-0003, and WT_Ciprofloxacin with TM_Ciprofloxacin revealed that these complexes occupy significantly less space, indicating enhanced protein stability. The ligand binding contributes to the

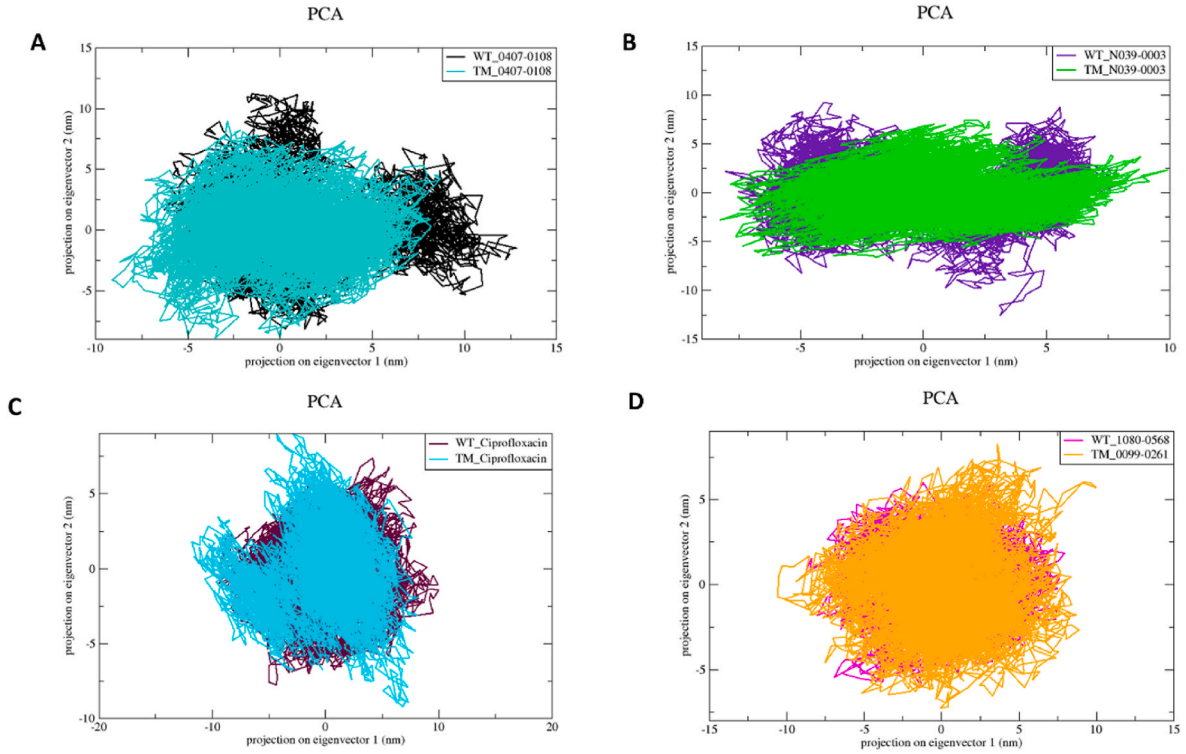

Fig. 9. PCA analysis of all complexes. A) Comparative PCA graph of WT and TM with ligand 0407–0108, B) Comparative PCA graph of WT and TM with ligand N039–0003, C) Comparative PCA graph of WT and TM with Ciprofloxacin, D) Comparative PCA graph of WT with ligand 1080–0568 and TM with ligand 0099–0261.

stability of both WT and TM proteins. Similarly, the complexes WT_1080–0568 and TM_0099–0261 also exhibited confined projections, occupying less space in the trajectory plot, which further indicates increased stability.

3.5.7. Free energy landscape (FEL) analysis

The FEL analysis is crucial for examining the protein's transition, stability, and conformation following ligand binding. A lower transition state and minimum global energy signify enhanced protein stability upon ligand binding. Fig. 10 illustrates the FEL analysis for all complexes. The trajectory analysis of the WT_0407–0108 complex reveals multiple transition states with several global energy minima, including one with a minimum global energy and another with an intermediate global energy. In contrast, the FEL analysis of the TM_0407–0108 complex shows a single transition state with a minimum global energy. For the WT_N039-0003 complex, multiple transition states were observed, with global energies ranging from minimum to intermediate. Conversely, the TM_N039-0003 complex exhibited a clustered energy landscape with a single transition state and minimum global energy. The global energy landscape of the WT_Ciprofloxacin complex displayed a clustered single transition state with global energies ranging from minimum to intermediate. In contrast, the TM_Ciprofloxacin complex showed multiple transition states with global energies ranging from minimum to intermediate. The FEL analysis of the WT_0108–0568 complex exhibited a clustered energy landscape with a single transition state and global energies ranging from minimum to intermediate. Similarly, the TM_0099–0261 complex showed a single transition state with global energies ranging from minimum to intermediate.

3.5.8. Dynamic cross-correlation matrix (DCCM)

The DCCM provides insights into the time-correlated movements of amino acid residues after ligand binding. Bright colors (red-green) with minimal deviation in residue motion indicate a positive correlation, while the opposite suggests a negative correlation. The DCCM analysis of WT_0407–0108, TM_0407–0108, WT_N039-0003, TM_N039-0003, WT_Ciprofloxacin, and TM_Ciprofloxacin showed positive correlation and self-correlation, with slight motion deviations ranging from 0 (red) to 0.75 nm (green) at residue indices 50–100, 260–300, and 400–500. This indicates consistent and synchronized movements among the amino acid residues. Similarly, the DCCM analysis of complexes WT_1080–0568 and TM_0099–0261 also exhibited self-positive correlation, with minimal motion deviations in the same residue index ranges (50–100, 260–300, and 400–500), showing distances of 0–0.75 nm. These findings are illustrated in Fig. 11, depicting the DCCM analysis of all complexes.

3.6. Molecular Mechanics Poisson-Boltzmann Surface Area (MMPBSA) analysis

MMPBSA is a sophisticated computational technique used to estimate the total binding free energy, encompassing the covalent interactions between proteins and ligands in solution. The MMPBSA analysis of the complexes WT_0407–0108, WT_N039-0003, WT_1080–0568, WT_Ciprofloxacin, TM_0407–0108, TM_N039-0003, TM_0099–0261, and TM_Ciprofloxacin provides deeper insights into their binding specificities, affinities, and covalent interactions. A comparative MMPBSA analysis of the WT_0407–0108 and TM_0407–0108 complexes revealed total binding energies of 7.547 ± 10.308 kJ/mol and −40.809 ± 11.733 kJ/mol, respectively. Similarly, the total binding energies for the WT_N039-0003 and TM_N039-0003 complexes were −125.773 ± 73.415 kJ/mol and −95.386 ± 128.887 kJ/mol, respectively. The WT_Ciprofloxacin and TM_Ciprofloxacin complexes exhibited total binding energies of 15.785 ± 44.616 kJ/mol and −102.903 ± 17.168 kJ/mol, respectively. Furthermore, the MMPBSA analysis of the WT-1080-0568 and TM-0099-0261 complexes showed total binding free energies of −221.437 ± 112.074 kJ/mol and 14.427 ± 79.492 kJ/mol, respectively. Table 5 presents the MMPBSA results, detailing the contributions of various energy components to the total binding free energy of all complexes.

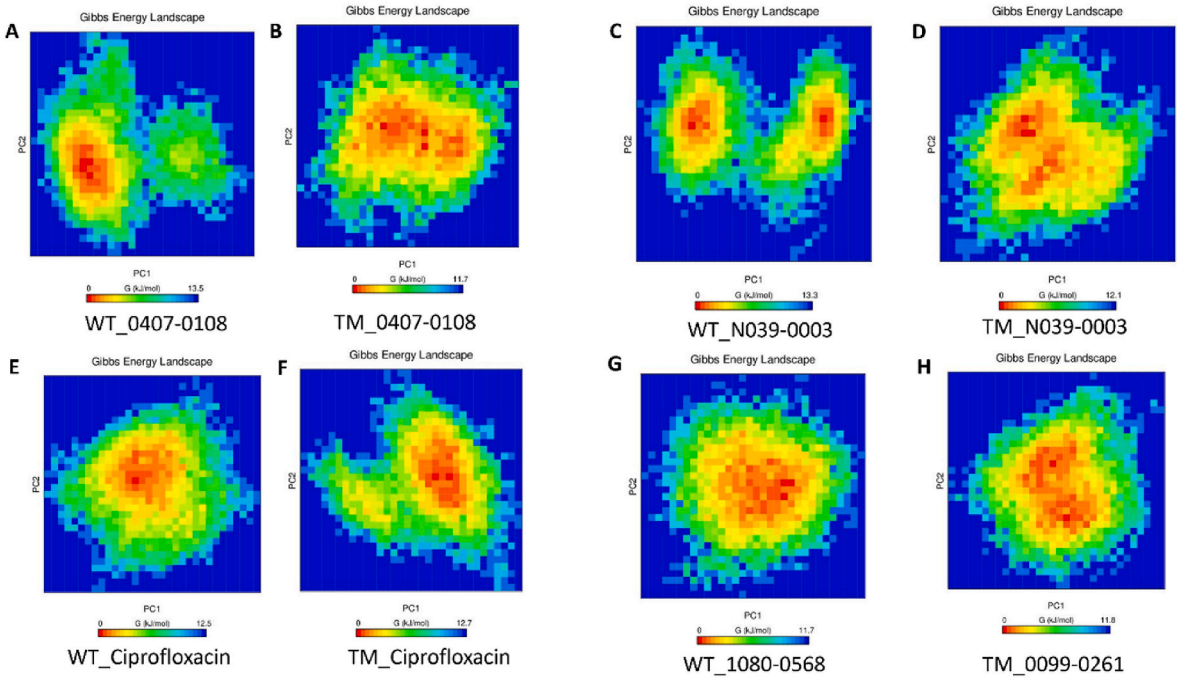

Fig. 10. Free energy landscape analysis of all complexes. Gibbs energy landscape of A) WT with ligand 0407–0108, B) TM with ligand 0407–0108, C) WT with ligand N039-0003, D) TM with ligand N039-0003, E) WT with Ciprofloxacin, F) TM with Ciprofloxacin, G) WT with ligand 1080–0568 and H) TM with ligand 0099–0261.

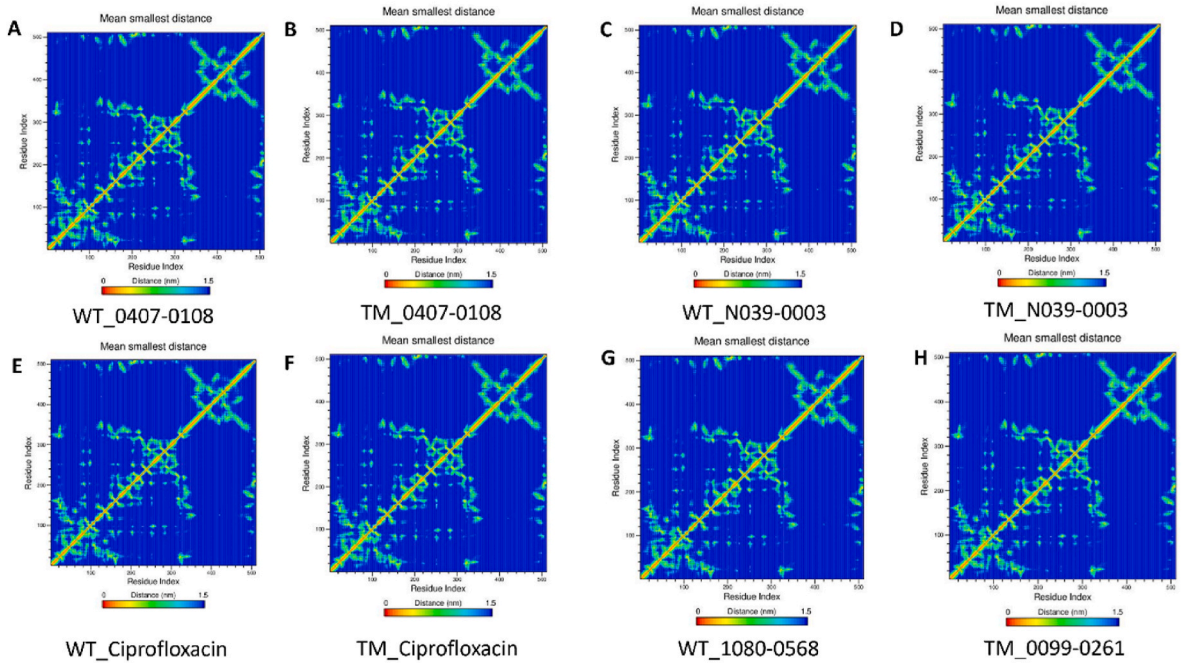

Fig. 11. Dynamic cross-correlation matrix analysis of all complexes. The correlation matrix of A) WT with ligand 0407–0108, B) TM with ligand 0407–0108, C) WT with ligand N039-0003, D) TM with ligand N039-0003, E) WT with Ciprofloxacin, F) TM with Ciprofloxacin, G) WT with ligand 1080–0568 and H) TM with ligand 0099–0261.

Table 5
Overview of MM-PBSA analysis of top 4 natural compounds and ciprofloxacin in complex with wild type and triple mutant DNA Gyrase A protein of *Salmonella typhimurium*.

Targeted protein	Natural compounds	Van der Waal Energy (kJ/mol)	Electrostatic Energy (kJ/mol)	Polar Solvation Energy (kJ/mol)	SASA Energy (kJ/mol)	Total Binding Energy (kJ/mol)
Wild type	0407–0108	−83.121±9.857	−84.888±15.569	189.074±17.694	−13.517±0.492	7.547±10.308
	N039-0003	−0.168±0.248	−168.188±53.552	42.729±59.031	−0.147±1.390	−125.773±73.415
	1080–0568	−58.733±12.731	−250.318±139.655	96.330±102.955	−8.716±1.475	−221.437±112.074
	Ciprofloxacin	−3.070±4.740	2.853±32.383	18.223±63.794	−2.221±2.050	15.785±44.616
Triple mutant	0407–0108	−92.267±7.367	−52.057±17.343	115.472±30.463	−11.956±0.400	−40.809±11.733
	N039-0003	−0.017±0.018	−105.977±32.427	11.312± 27.285	−0.703±1.403	−95.386±128.887
	0099–0261	−0.003±0.001	−0.712±1.311	15.731±79.915	−0.590±0.805	14.427±79.492
	Ciprofloxacin	−85.490±9.401	−264.768±67.171	258.434±75.498	−11.079±1.367	−102.903±17.168

4. Discussion

In many developing and industrialized nations, the escalating drug resistance in *S.* Typhimurium has emerged as a significant health concern due to its high worldwide morbidity rate. A multitude of studies have highlighted the rise of Multi-Drug Resistant (MDR) strains of *S.* Typhimurium, primarily attributed to the extended and indiscriminate use of antibiotics. From 1969 to 2006, research documented the pathogen's resistance to several first-generation antibiotics, including ampicillin, trimethoprim, tetracycline, and chloramphenicol. Fluoroquinolones were initially the antibiotics of choice for severe gastroenteritis and bacteremia caused by *S.* Typhimurium, owing to their efficacy in treating such infections [46]. However, it is now advised to refrain from prescribing third-generation or fluoroquinolone antibiotics for *Salmonella*-related gastroenteritis unless the disease is severe or exacerbates the patient's condition, as most cases are self-limiting [47]. Fluoroquinolones work by inhibiting DNA synthesis and disrupting the activity of DNA gyrase and topoisomerase IV, thereby limiting *Salmonella*'s survival. The mid-2000s and 2010s saw the emergence of second and third-generation antibiotics like sulphonamides, cefotaxime, ciprofloxacin, and nalidixic acid due to increased and unregulated antibiotic use even for mild *Salmonella* infection [5]. Reports of chromosomal and plasmid-associated resistance development against fluoroquinolone in *S.* Typhimurium emerged primarily due to mutations in the active binding site of DNA gyrase and topoisomerase IV. Globally, mutations at positions 83 and 87 of the *gyrA* gene in *S.* Typhimurium isolates were observed, resulting in amino acid changes such as SER83PHE and ASP87GLY/ASN. Other DNA gyrase and topoisomerase IV subunits, such as *gyrB*, *parC*, and *parE*, also exhibited mutations or remained unchanged, depending on geographical origin and host. The selective antibiotic pressure on the DNA gyrase led to acquisition of single point mutation at 83 of *gyrA*, expressing low resistance to ciprofloxacin of MIC 0.25 mg/L. Additionally the acquisition of second mutation in *parC* at 80 from serine to isoleucine exhibited intermediate ciprofloxacin resistance with MIC ranging from 4 mg/L to 256 mg/L with no futher mutational gain in other subunits of DNA gyrase [48]. Meanwhile the TM in *gyrA* of middle eastern strain showed high ciprofloxacin resistance with MIC of 512 mg/L with no additional mutation in other subunits of DNA gyrase [18].

A recent study by Kakatkar et al. (2021) explored the development of antibiotic resistance in *S.* Typhimurium due to extended exposure to high ciprofloxacin doses. The study identified approximately 40,513 mutations through whole genome analysis, including point mutations in critical genes like *gyrA* and changes in metabolic pathways due to antibiotic pressure. While additional mutations in genes such as *gyrB, parC, parE, rpoB*, and iron, coupled with extensive metabolic pathway

changes, did not directly contribute to fluoroquinolone resistance, they did assist in maintaining homeostasis [49]. The presence of a TM solely in the DNA gyrase subunit A suggests that strains with these mutations can readily adapt, even by intermediate or fluoroquinolone-sensitive strains, as no further mutations are required in other subunits to stabilize the DNA gyrase A subunit protein and maintain homeostasis. In our study, mutational analysis of the TM DNA gyrase A subunit in *Salmonella* Typhimurium using DDMut revealed that only the Ser83Phe point mutation stabilized the protein.

Conversely, other point mutations led to protein destabilization. This indicates that the DNA gyrase A subunit protein unfolded and became more flexible due to the triple mutation. Understanding the combined effect of these mutations on the protein is crucial, as it likely caused a significant conformational change in the TM protein, potentially increasing its resistance to fluoroquinolones. The spread of *gyrA* TM *Salmonella* Typhimurium strains could pose a severe threat in the future, underscoring the importance of finding a potent natural compound capable of inhibiting both WT and TM GyrA protein in *S.* Typhimurium.

In recent years, the utilization of natural compounds derived from drug-like small molecules has surged due to their structural and chemical diversity. When combined with advanced computational approaches such as virtual screening and molecular dynamics, drug discovery becomes more efficient, accurate, and rapid in screening and optimizing these compounds [50,51]. The computational approach in drug discovery offers the advantage of early toxicity prediction using cutting-edge, data-driven machine learning models and algorithms, including neural networks and mathematical modeling, to predict the pharmacodynamics and pharmacokinetics of the screened molecules precisely. This enables the identification of harmful effects of compounds at the initial stages of drug discovery, making the process cost-effective and efficient [52–54].

Consequently, these computational techniques have emerged as a promising strategy for identifying unique lead molecules with high therapeutic potential against bacterial pathogens like *Salmonella*. Our advanced computational virtual screening and docking studies identified four natural compounds from the ChemDiv database: CID: 0407–0108, N039-0003, 1080–0568, and 0099–0261. These compounds exhibited exceptional physicochemical properties and docking scores higher than the control drug ciprofloxacin with WT and TM DNA gyrase subunit A. Trajectory analyses of simulated complexes provide deeper insights into the dynamic behavior of the protein-ligand complex and the impact of ligand binding to the protein [55]. RMSD assesses the deviation of proteins, protein-ligand complexes, or ligands from their primary reference structure [56]. RMSD analysis of the protein-ligand complexes showed that the average RMSD values of all WT complexes were higher than those for the TM complexes, indicating better drug binding and structural stability. RMSF analysis revealed significant flexibility and fluctuations [57] in residues near the 237th, 260th-300th positions, as well as from the 360th-400th and around the 500th position. Although certain complexes (WT_0407–0108, TM_N039-0003, and WT_1080–0568) showed high fluctuation around the 100th residue, it was minor in others. This variation could be attributed to the presence or absence of TM near the 100th position combined with the effect of ligand binding on nearby residues. The roles of these residues are crucial as they may influence protein structure and function, potentially impacting drug resistance mechanisms. Determining the Rg values in protein-ligand complexes is essential for understanding conformational flexibility and the dynamics of protein folding and unfolding [58]. Further determination of the Rg values indicated that TM with top-hit ligands exhibited tighter binding and higher stability than WT with top-hit ligands. SASA analysis assesses the contribution of protein active sites to solvent effects in the environment [59]. SASA analysis indicated greater surface area accessibility and solvent interaction for WT and TM proteins when complexed with their respective ligands. TM with top ligands showed marginally higher SASA values.

H-bond analysis is crucial for evaluating the structural stability and interaction dynamics [60] between WT and TM proteins with their respective ligands. The analysis revealed that ciprofloxacin formed a greater number of H-bonds with both WT and TM proteins compared to other ligands. However, its binding energy and affinity were significantly lower than those of the potent lead molecules identified in this study. PCA was employed to calculate the variances in variables derived from fundamental components [61], aiding in the comprehension of the dynamic motion complexity in protein-ligand complexes, which is related to protein folding and stability. The thermodynamic aspects of ligand binding at the atomic level were examined using FEL analysis [55]. Both PCA and FEL analyses confirmed the stability of TM when complexed with top-hit ligands, suggesting that these ligands are more feasible and spontaneous for binding. DCCM analysis, which is based on time correlation and covariance from simulated target proteins, graphically depicted the collective fluctuations in residue motions [62]. This analysis revealed positive correlations in all complexes, indicating effective ligand binding to both WT and TM proteins. MM-PBSA analysis was utilized to calculate the contributions of various energy components, such as van der Waals and electrostatic interactions, to the total binding free energy of the ligand towards the protein [63]. The MM-PBSA analysis indicated that ligand N039-0003 exhibited high total binding energy towards both WT and TM proteins, identifying it as a potent lead compound. A limitation of this study is its reliance on computational methods, necessitating validation of the results through *in vitro* and *in vivo* experiments. Further research is required to investigate the pharmacokinetics, toxicity, and efficacy of the identified compounds in clinical settings.

5. Conclusion

Fluoroquinolone-resistant *S.* Typhimurium, especially with a triple mutation in DNA gyrase A, poses a serious global health threat. Our mutational stability analysis revealed that the triple mutation in DNA gyrase A of *S.* Typhimurium led to a conformational protein change, developing high resistance to fluoroquinolone drugs. Our study findings unveiled that natural compounds from the ChemDiv database, such as 0407–0108, N039-0003, 1080–0568, and 0099–0261, were identified to be potent DNA gyrase A inhibitors based on virtual screening, ADME/T studies, and dynamics studies. These compounds exhibited higher affinity and binding energy towards WT and TM DNA gyrase A than the conventional fluoroquinolone drug ciprofloxacin, laying the groundwork for future drug development and therapeutic strategies.

CRediT authorship contribution statement

Sree Haryini: Writing – original draft, Visualization, Validation, Software, Methodology, Investigation, Conceptualization. **George Priya Doss C:** Writing – review & editing, Visualization, Supervision, Project administration, Methodology, Conceptualization.

Declaration of competing interest

No conflict of interest exists.

Acknowledgments

The authors would like to take this opportunity to thank the management of Vellore Institute of Technology (VIT), Vellore, India, for providing the necessary facilities and encouragement to carry out this work.

Appendix A. Supplementary data

Supplementary data to this article can be found online at https://doi.org/10.1016/j.bbrep.2024.101901.

Data availability

The data presented in this study are available in the present article and supplementary material.

References

[1] J. Fierer, Invasive non-typhoidal Salmonella (iNTS) infections, Clin. Infect. Dis. 75 (2022) 732–738, https://doi.org/10.1093/cid/ciac035.

[2] G.L. Popa, M.I. Papa, Salmonella spp. infection - a continuous threat worldwide, Germs 11 (2021) 88–96, https://doi.org/10.18683/germs.2021.1244.

[3] Food safety management. https://shop.elsevier.com/books/food-safety-management/andersen/978-0-12-820013-1, 2023. (Accessed 28 November 2024).

[4] S. Lund, M. Tahir, L.I. Vohra, A.H. Hamdana, S. Ahmad, Outbreak of monophasic Salmonella Typhimurium Sequence Type 34 linked to chocolate products, Ann Med Surg (Lond) 82 (2022) 104597, https://doi.org/10.1016/j.amsu.2022.104597.

[5] S.D. Patra, N.K. Mohakud, R.K. Panda, B.R. Sahu, M. Suar, Prevalence and multidrug resistance in Salmonella enterica typhimurium: an overview in south East asia, World J. Microbiol. Biotechnol. 37 (2021) 185, https://doi.org/10.1007/s11274-021-03146-8.

[6] J.J. Jacob, D. Solaimalai, D.P. Muthuirulandi Sethuvel, T. Rachel, P. Jeslin, S. Anandan, B. Veeraraghavan, A nineteen-year report of serotype and antimicrobial susceptibility of enteric non-typhoidal Salmonella from humans in Southern India: changing facades of taxonomy and resistance trend, Gut Pathog. 12 (2020) 49, https://doi.org/10.1186/s13099-020-00388-z.

[7] X. Qin, M. Yang, H. Cai, Y. Liu, L. Gorris, M.Z. Aslam, K. Jia, T. Sun, X. Wang, Q. Dong, Antibiotic resistance of Salmonella typhimurium monophasic variant 1,4,[5],12:i:-in China: a systematic review and meta-analysis, Antibiotics 11 (2022) 532, https://doi.org/10.3390/antibiotics11040532.

[8] X. Wang, S. Biswas, N. Paudyal, H. Pan, X. Li, W. Fang, M. Yue, Antibiotic resistance in Salmonella typhimurium isolates recovered from the food chain through national antimicrobial resistance monitoring system between 1996 and 2016, Front. Microbiol. 10 (2019). https://www.frontiersin.org/articles/10.3389/fmicb.2019.00985. (Accessed 30 January 2024).

[9] T.D.M. Pham, Z.M. Ziora, M.A.T. Blaskovich, Quinolone antibiotics, Medchemcomm 10 (2019) 1719–1739, https://doi.org/10.1039/c9md00120d.

[10] J. Li, H. Hao, A. Sajid, H. Zhang, Z. Yuan, J. Li, H. Hao, A. Sajid, H. Zhang, Z. Yuan, Fluoroquinolone resistance in *Salmonella*: mechanisms, fitness, and virulence, in: Salmonella - A Re-emerging Pathogen, IntechOpen, 2018, https://doi.org/10.5772/intechopen.74699.

[11] P. Heisig, High-level fluoroquinolone resistance in a Salmonella typhimurium isolate due to alterations in both gyrA and gyrB genes, J. Antimicrob. Chemother. 32 (1993) 367–377, https://doi.org/10.1093/jac/32.3.367.

[12] D.C. Hooper, G.A. Jacoby, Topoisomerase inhibitors: fluoroquinolone mechanisms of action and resistance, Cold Spring Harb Perspect Med 6 (2016) a025320, https://doi.org/10.1101/cshperspect.a025320.

[13] A. Fàbrega, S. Madurga, E. Giralt, J. Vila, Mechanism of action of and resistance to quinolones, Microb. Biotechnol. 2 (2009) 40–61, https://doi.org/10.1111/j.1751-7915.2008.00063.x.

[14] X. Yang, S. Yang, S. Liu, S. Liu, J. Zhang, W. Guo, J. Wang, Z. Song, L. Xue, M. Chen, S. Wu, X. Wei, Q. Wu, Characterization of quinolone resistance in *Salmonella enterica* serovar Typhimurium and its monophasic variants from food and patients in China, Journal of Global Antimicrobial Resistance 35 (2023) 216–222, https://doi.org/10.1016/j.jgar.2023.09.010.

[15] B. Yang, M. Xi, S. Cui, X. Zhang, J. Shen, M. Sheng, D. Qu, X. Wang, J. Meng, Mutations in gyrase and topoisomerase genes associated with fluoroquinolone resistance in *Salmonella* serovars from retail meats, Food Res. Int. 45 (2012) 935–939, https://doi.org/10.1016/j.foodres.2011.01.031.

[16] D.J. Eaves, L. Randall, D.T. Gray, A. Buckley, M.J. Woodward, A.P. White, L.J. V. Piddock, Prevalence of mutations within the quinolone resistance-determining region of gyrA, gyrB, parC, and parE and association with antibiotic resistance in quinolone-resistant Salmonella enterica, Antimicrob. Agents Chemother. 48 (2004) 4012–4015, https://doi.org/10.1128/AAC.48.10.4012-4015.2004.

[17] R. Gaind, B. Paglietti, M. Murgia, R. Dawar, S. Uzzau, P. Cappuccinelli, M. Deb, P. Aggarwal, S. Rubino, Molecular characterization of ciprofloxacin-resistant Salmonella enterica serovar Typhi and Paratyphi A causing enteric fever in India, J. Antimicrob. Chemother. 58 (2006) 1139–1144, https://doi.org/10.1093/jac/dkl391.

[18] AA Rushdy, MI Mabrouk, FAH Abu-Sef, ZH Kheiralla, SMA All, NM Saleh, Contribution of different mechanisms to the resistance to fluoroquinolones in clinical isolates of Salmonella enterica, The Brazilian Journal of Infectious Diseases 17 (4) (2013) 431–437. https://doi.org/10.1016/j.bjid.2012.11.01.

[19] N. Dong, Y. Li, J. Zhao, H. Ma, J. Wang, B. Liang, X. Du, F. Wu, S. Xia, X. Yang, H. Liu, C. Yang, S. Qiu, H. Song, L. Jia, Y. Li, Y. Sun, The phenotypic and molecular characteristics of antimicrobial resistance of Salmonella enterica subsp. enterica serovar Typhimurium in Henan Province, China, BMC Infect. Dis. 20 (2020) 511, https://doi.org/10.1186/s12879-020-05203-3.

[20] S. Kariuki, M.A. Gordon, N. Feasey, C.M. Parry, Antimicrobial resistance and management of invasive Salmonella disease, Vaccine 33 (2015) C21–C29, https://doi.org/10.1016/j.vaccine.2015.03.102.

[21] A.G. Atanasov, S.B. Zotchev, V.M. Dirsch, C.T. Supuran, Natural products in drug discovery: advances and opportunities, Nat. Rev. Drug Discov. 20 (2021) 200–216, https://doi.org/10.1038/s41573-020-00114-z.

[22] J.M. Al-Khayri, R. Rashmi, V. Toppo, P.B. Chole, A. Banadka, W.N. Sudheer, P. Nagella, W.F. Shehata, M.Q. Al-Mssallem, F.M. Alessa, M.I. Almaghasla, A.A.-S. Rezk, Plant secondary metabolites: the weapons for biotic stress management, Metabolites 13 (2023) 716, https://doi.org/10.3390/metabo13060716.

[23] Chemical Libraries. Complete List of ChemDiv's Compound Libraries, (n.d.). https://www.chemdiv.com/catalog/complete-list-of-compounds-libraries/(accessed December 2, 2024).

[24] The universal protein resource (UniProt), Nucleic Acids Res. 36 (2008) D190–D195, https://doi.org/10.1093/nar/gkm895.

[25] S. Kim, E.E. Bolton, PubChem: a large-scale public chemical database for drug discovery, in: Open Access Databases and Datasets for Drug Discovery, John Wiley & Sons, Ltd, 2024, pp. 39–66, https://doi.org/10.1002/9783527830497.ch2.

[26] X. Robin, A.M. Waterhouse, S. Bienert, G. Studer, L.T. Alexander, G. Tauriello, T. Schwede, J. Pereira, The SWISS-model repository of 3D protein structures and models, in: Open Access Databases and Datasets for Drug Discovery, John Wiley & Sons, Ltd, 2024, pp. 175–199, https://doi.org/10.1002/9783527830497.ch6.

[27] H.M. Berman, J. Westbrook, Z. Feng, G. Gilliland, T.N. Bhat, H. Weissig, I. N. Shindyalov, P.E. Bourne, The protein Data Bank, Nucleic Acids Res. 28 (2000) 235–242, https://doi.org/10.1093/nar/28.1.235.

[28] J. Jumper, R. Evans, A. Pritzel, T. Green, M. Figurnov, O. Ronneberger, K. Tunyasuvunakool, R. Bates, A. Žídek, A. Potapenko, A. Bridgland, C. Meyer, S.A. A. Kohl, A.J. Ballard, A. Cowie, B. Romera-Paredes, S. Nikolov, R. Jain, J. Adler, T. Back, S. Petersen, D. Reiman, E. Clancy, M. Zielinski, M. Steinegger, M. Pacholska, T. Berghammer, S. Bodenstein, D. Silver, O. Vinyals, A.W. Senior, K. Kavukcuoglu, P. Kohli, D. Hassabis, Highly accurate protein structure prediction with AlphaFold, Nature 596 (2021) 583–589, https://doi.org/10.1038/s41586-021-03819-2.

[29] S. Sasidharan, P. Saudagar, Chapter 23 - prediction, validation, and analysis of protein structures: a beginner's guide, in: T. Tripathi, V.K. Dubey (Eds.), Advances in Protein Molecular and Structural Biology Methods, Academic Press, 2022, pp. 373–385, https://doi.org/10.1016/B978-0-323-90264-9.00023-4.

[30] T.A. Halgren, R.B. Murphy, R.A. Friesner, H.S. Beard, L.L. Frye, W.T. Pollard, J. L. Banks, Glide: a new approach for rapid, accurate docking and scoring. 2. Enrichment factors in database screening, J. Med. Chem. 47 (2004) 1750–1759, https://doi.org/10.1021/jm030644s.

[31] A. Ghosh, S. N, S. Saha, Survey of drug resistance associated gene mutations in Mycobacterium tuberculosis, ESKAPE and other bacterial species, Sci. Rep. 10 (2020) 8957, https://doi.org/10.1038/s41598-020-65766-8.

[32] D.M. Faiza, Performing in silico mutagenesis using Pymol? Bioinformatics Review (2021). https://bioinformaticsreview.com/20211120/performing-in-silico-mutagenesis-using-pymol/. (Accessed 31 January 2024).

[33] Y. Zhou, Q. Pan, D.E.V. Pires, C.H.M. Rodrigues, D.B. Ascher, DDMut: predicting effects of mutations on protein stability using deep learning, Nucleic Acids Res. 51 (2023) W122–W128, https://doi.org/10.1093/nar/gkad472.

[34] QikProp, Schrödinger (n.d.). https://www.schrodinger.com/platform/products/qikprop/(accessed August 17, 2024).

[35] W. Tian, C. Chen, X. Lei, J. Zhao, J. Liang, CASTp 3.0: computed atlas of surface topography of proteins, Nucleic Acids Res. 46 (2018) W363–W367, https://doi.org/10.1093/nar/gky473.

[36] R.A. Friesner, R.B. Murphy, M.P. Repasky, L.L. Frye, J.R. Greenwood, T.A. Halgren, P.C. Sanschagrin, D.T. Mainz, Extra precision glide: docking and scoring incorporating a model of hydrophobic enclosure for Protein−Ligand complexes, J. Med. Chem. 49 (2006) 6177–6196, https://doi.org/10.1021/jm051256o.

[37] E.C. Meng, T.D. Goddard, E.F. Pettersen, G.S. Couch, Z.J. Pearson, J.H. Morris, T. E. Ferrin, UCSF ChimeraX: tools for structure building and analysis, Protein Sci. 32 (2023) e4792, https://doi.org/10.1002/pro.4792.

[38] M.J. Abraham, T. Murtola, R. Schulz, S. Páll, J.C. Smith, B. Hess, E. Lindahl, GROMACS: high performance molecular simulations through multi-level parallelism from laptops to supercomputers, SoftwareX 1–2 (2015) 19–25, https://doi.org/10.1016/j.softx.2015.06.001.

[39] S. Jo, T. Kim, V.G. Iyer, W. Im, CHARMM-GUI: a web-based graphical user interface for CHARMM, J. Comput. Chem. 29 (2008) 1859–1865, https://doi.org/10.1002/jcc.20945.

[40] J. Lee, X. Cheng, J.M. Swails, M.S. Yeom, P.K. Eastman, J.A. Lemkul, S. Wei, J. Buckner, J.C. Jeong, Y. Qi, S. Jo, V.S. Pande, D.A. Case, C.L.I. Brooks, A.D. Jr. MacKerell, J.B. Klauda, W. Im, CHARMM-GUI input generator for NAMD, GROMACS, AMBER, OpenMM, and CHARMM/OpenMM simulations using the CHARMM36 additive force field, J. Chem. Theor. Comput. 12 (2016) 405–413, https://doi.org/10.1021/acs.jctc.5b00935.

[41] C.C. David, D.J. Jacobs, Principal component analysis: a method for determining the essential dynamics of proteins, in: D.R. Livesay (Ed.), Protein Dynamics: Methods and Protocols, Humana Press, Totowa, NJ, 2014, pp. 193–226, https://doi.org/10.1007/978-1-62703-658-0_11.

[42] I. Tavernelli, S. Cotesta, E.E. Di Iorio, Protein dynamics, thermal stability, and free-energy landscapes: a molecular dynamics investigation, Biophys. J. 85 (2003) 2641–2649, https://doi.org/10.1016/S0006-3495(03)74687-6.

[43] P.H. Hünenberger, A.E. Mark, W.F. van Gunsteren, Fluctuation and cross-correlation analysis of protein motions observed in nanosecond molecular dynamics simulations, J. Mol. Biol. 252 (1995) 492–503, https://doi.org/10.1006/jmbi.1995.0514.

[44] R. Kumari, R. Kumar, A. Lynn, g_mmpbsa—a GROMACS tool for high-throughput MM-PBSA calculations, J. Chem. Inf. Model. 54 (2014) 1951–1962, https://doi.org/10.1021/ci500020m.

[45] M.S. Valdés-Tresanco, M.E. Valdés-Tresanco, P.A. Valiente, E. Moreno, gmx_MMPBSA: a new tool to perform end-state free energy calculations with

GROMACS, J. Chem. Theor. Comput. 17 (2021) 6281–6291, https://doi.org/10.1021/acs.jctc.1c00645.
[46] L.J.V. Piddock, Fluoroquinolone resistance in Salmonella serovars isolated from humans and food animals 1, FEMS (Fed. Eur. Microbiol. Soc.) Microbiol. Rev. 26 (2002) 3–16, https://doi.org/10.1111/j.1574-6976.2002.tb00596.x.
[47] D.H. Hamer, S.L. Gorbach, Chapter 10 - use of the quinolones for treatment and prophylaxis of bacterial gastrointestinal infections, in: V.T. Andriole (Ed.), The Quinolones, third ed., Academic Press, San Diego, 2000, pp. 303–323, https://doi.org/10.1016/B978-012059517-4/50011-8.
[48] A. Shaheen, A. Tariq, M. Iqbal, O. Mirza, A. Haque, T. Walz, M. Rahman, Mutational diversity in the quinolone resistance-determining regions of type-II topoisomerases of Salmonella serovars, Antibiotics 10 (2021) 14–55, https://doi.org/10.3390/antibiotics10121455.
[49] A.S. Kakatkar, A. Das, R. Shashidhar, Ciprofloxacin induced antibiotic resistance in Salmonella Typhimurium mutants and genome analysis, Arch. Microbiol. 203 (2021) 6131–6142, https://doi.org/10.1007/s00203-021-02577-z.
[50] Integration of target discovery, drug discovery and drug delivery: A review on computational strategies - Duarte - 2019 - WIREs Nanomedicine and Nanobiotechnology - Wiley Online Library, (n.d.). https://wires.onlinelibrary.wiley.com/doi/abs/10.1002/wnan.1554 (accessed December 2, 2024).
[51] X. Lin, X. Li, X. Lin, A review on applications of computational methods in drug screening and design, Molecules 25 (2020) 1375, https://doi.org/10.3390/molecules25061375.
[52] M. Roney, M.F.F. Mohd Aluwi, The importance of in-silico studies in drug discovery, Intelligent Pharmacy 2 (2024) 578–579, https://doi.org/10.1016/j.ipha.2024.01.010.
[53] E.P. Chen, S. Dutta, M.-H. Ho, M.P. DeMartino, Model-based virtual PK/PD exploration and machine learning approach to define PK drivers in early drug discovery, J. Med. Chem. 67 (2024) 3727–3740, https://doi.org/10.1021/acs.jmedchem.3c02169.
[54] K. Wu, X. Li, Z. Zhou, Y. Zhao, M. Su, Z. Cheng, X. Wu, Z. Huang, X. Jin, J. Li, M. Zhang, J. Liu, B. Liu, Predicting pharmacodynamic effects through early drug discovery with artificial intelligence-physiologically based pharmacokinetic (AI-PBPK) modelling, Front. Pharmacol. 15 (2024), https://doi.org/10.3389/fphar.2024.1330855.
[55] N. Wu, R. Zhang, X. Peng, L. Fang, K. Chen, J.S. Jestilä, Elucidation of protein–ligand interactions by multiple trajectory analysis methods, Phys. Chem. Chem. Phys. 26 (2024) 6903–6915, https://doi.org/10.1039/D3CP03492E.
[56] Y. Maruyama, R. Igarashi, Y. Ushiku, A. Mitsutake, Analysis of protein folding simulation with moving Root mean square deviation, J. Chem. Inf. Model. 63 (2023) 1529–1541, https://doi.org/10.1021/acs.jcim.2c01444.
[57] M. De Vivo, M. Masetti, G. Bottegoni, A. Cavalli, Role of molecular dynamics and related methods in drug discovery, J. Med. Chem. 59 (2016) 4035–4061, https://doi.org/10.1021/acs.jmedchem.5b01684.
[58] M.Yu Lobanov, N.S. Bogatyreva, O.V. Galzitskaya, Radius of gyration as an indicator of protein structure compactness, Mol. Biol. 42 (2008) 623–628, https://doi.org/10.1134/S0026893308040195.
[59] J.A. Marsh, S.A. Teichmann, Relative solvent accessible surface area predicts protein conformational changes upon binding, Structure 19 (2011) 859–867, https://doi.org/10.1016/j.str.2011.03.010.
[60] D. Chen, N. Oezguen, P. Urvil, C. Ferguson, S.M. Dann, T.C. Savidge, Regulation of protein-ligand binding affinity by hydrogen bond pairing, Sci. Adv. 2 (2016) e1501240, https://doi.org/10.1126/sciadv.1501240.
[61] M. Greenacre, P.J.F. Groenen, T. Hastie, A.I. D'Enza, A. Markos, E. Tuzhilina, Principal component analysis, Nat Rev Methods Primers 2 (2022) 1–21, https://doi.org/10.1038/s43586-022-00184-w.
[62] T. Ichiye, M. Karplus, Collective motions in proteins: a covariance analysis of atomic fluctuations in molecular dynamics and normal mode simulations, Proteins: Struct., Funct., Bioinf. 11 (1991) 205–217, https://doi.org/10.1002/prot.340110305.
[63] C. Wang, P.H. Nguyen, K. Pham, D. Huynh, T.-B. Nancy Le, H. Wang, P. Ren, R. Luo, Calculating protein-ligand binding affinities with MMPBSA: method and error analysis, J. Comput. Chem. 37 (2016) 2436–2446, https://doi.org/10.1002/jcc.24467.